The Multiscale Bowler-Hat Transform
for Blood Vessel Enhancement in Retinal Images

Çiğdem Sazak[a], Carl J. Nelson[b], Boguslaw Obara[a,*]

[a]*Department of Computer Science, Durham University, UK*
[b]*School of Physics and Astronomy, Glasgow University, UK*

Abstract

Enhancement, followed by segmentation, quantification and modelling of blood vessels in retinal images plays an essential role in computer-aided retinopathy diagnosis. In this paper, we introduce the bowler-hat transform method a new approach based on mathematical morphology for vessel enhancement. The proposed method combines different structuring elements to detect innate features of vessel-like structures. We evaluate the proposed method qualitatively and quantitatively and compare it with the state-of-the-art methods using both synthetic and real datasets. Our results establish that the proposed method achieves high-quality vessel-like structure enhancement in both synthetic examples and clinically relevant retinal images. The bowler-hat transform is shown to be able to detect fine vessels while still remaining robust at junctions.

Keywords: image enhancement, mathematical morphology, bowler-hat transform, blood vessel enhancement.

1. Introduction

Many biomedical images contain vessel-like structures, such as blood vessels or cytoskeletal networks [1]. Automated extraction of these structures and their connected network is often an essential step in quantitative image analysis and computer-aided diagnostic pipelines. For example, automated retinal vessel extraction is used for diagnosis, screening, and evaluation in a wide range of retinal diseases, including diabetes and arteriosclerosis [2].

However, for a multitude of reasons, *e.g.* noisy image capture, sample/patient variability, low contrast scenarios, etc., biomedical imaging modalities may suffer from poor quality. As such, standard image segmentation methods are not able to robustly detect vessel-like structures, and therefore some form of vessel-like structure enhancement is required [1].

A wide range of vessel enhancement methods have been proposed (see [2] and [1] for a recent review). These include Hessian [3, 4, 5], Phase Congruency Tensor [6, 7], mathematical morphology [8, 5, 9], adaptive histogram equalisation [10] based approaches and many others [11, 12, 13, 14, 15, 16, 17, 18].

However, many of these methods still have considerable issues when faced with variations in contrast, high levels of noise, variation in image features (*e.g.* lines vs junctions; retention of network connectivity), and complexity of method parameter space.

1.1. Contribution and Organisation

In this paper, we introduce a new enhancement method for vessel-like structures based on mathematical morphology, which exploits a key shape property of vessel-like structures: elongation. The proposed method, called the bowler-hat transform, has been qualitatively and quantitatively validated and compared with state-of-the-art methods using a range of synthetic data and publicly available retinal image datasets. The obtained results show that the proposed method achieves high-quality, vessel-like structure enhancement in both synthetic examples and clinically relevant retinal images. Retinal vessels can be considered at dark vessels on a bright background or, when the image is simply inverted, as bright vessels on a dark background. For the purposes of clarity in description and visualisation, we assume, and our methods work for, bright vessels on a dark background; this is similar to other methods [3]. The method is suitable for a range of biomedical image types without needing prior training or tuning. Finally, we have made the implementation of our approach available online, along with source code and all test functions. The rest of this paper is organised as follows. In Section 2, we introduce existing vessel-like structure enhancement methods and highlight their known limitations. Section 3 introduces and explains the proposed bowler-hat transform, Section 4 presents validation experiments and results on synthetic and real data. Finally, in Section 5, we discuss the results and future work.

---

*Corresponding author

Email address: `boguslaw.obara@durham.ac.uk` (Boguslaw Obara)

2. Related Work

In the following section we review existing approaches for vessel enhancement. We aim to highlight the positives and the negatives of these methods.

2.1. Multiscale Techniques for Image Processing

Multiscale image processing techniques are motivated by how the human visual system functions. In order to capture objects at both low and high spatial frequencies, images are processed at different scales either by altering the image size, *e.g.* in a Guassian pyramid, or by altering the filter size. By altering this scale in vessel enhancement different thickness vessels can be successfully enhanced.

In the first case, we are embedding the original image into a family of increasingly different scales, where the fine-scale details are successively suppressed. This multi-scale image representation is generally obtained by use of Gaussian filters or their derivatives defined at different scales, or by a use of mathematical morphology filters defined with a varying size of the structuring element.

Multiscale methods cover a wide range of approaches such as wavelets decomposition based methods, time evolving snakes, object tracking with increasing smoothing, fixed scale method [19], hierarchical approximation. There are many different fields definitions of the multiscale concepts, such as time [20, 21], information complexity [22], signal frequency [23] or smoothing degree [24], among others.

2.2. Hessian-based Methods

In [3], Frangi et al. introduce a novel Hessian-based multi-scale concept for 2D curvilinear/3D tubular structure enhancement in images. They construct the Hessian matrix using second-order Gaussian derivatives. The eigenvectors and eigenvalues of the Hessian matrix then define the principal directions of local image features. These can then be combined to form different measures of vesselness or blobness [1] in biomedical images.

2.2.1. Vesselness

The vesselness measure is proportional to the ratio of the eigenvalues [3]. If the magnitude of both eigenvalues is small, *i.e.* the local image structure is likely to be background, then the vesselness measure is small. If one eigenvalue is small and the other large then the local structure is likely to be vessel-like, and the vesselness measure is large. Finally, if both eigenvalues are high, then the structure is likely to be blob-like, and the vesselness measure is again small. Vesselness measurement is also regulated by two tunable thresholds which control the sensitivity of the line filter to the blob-like and tubular-like features.

This approach, however, leads to a failure at the intersection of vessels as both eigenvalues have similarly large values leading to a vesselness measure close to zero. Thus, vessel-like structures can be lost at junctions and therefore vessels network connectivity may be lost [25]. An extension of this approach can be found in [5] where a multi-scale morpho-Gaussian filter is combined with multi-scale

Hessian measurement to enhance the curvilinear features and reduce noise.

2.2.2. Neuriteness

As an alternative to vesselness, Meijering and colleagues introduce the neuriteness measure to enhance low contrast and highly inhomogeneous neurites in bioimages [26]. Using a modified Hessian, with a tuning parameter, and a different combination of eigenvalues, neuriteness infers a putative neurite in every pixel of the image that has a non-zero value. The second derivative reduces the approximation error of the first derivative. The local maximum where zero crossing of the first derivative, discovered with a negative value at the second order derivative.

A major failing for the neuriteness measure is that background noise signals are enhanced as if they are curvilinear structures. In the original paper [26] this is solved with a tracing stage; however, as an enhancer only, this can cause serious problems for further analysis. The neuriteness measure also leads to a failure at the intersection of vessels as both eigenvalues have similarly large values leading to a neuriteness measure close to zero. A further example of their work is found in [27].

2.2.3. Regularized Volume Ratio

Recently, Jerman and colleagues [28] propose a new Hessian-based vessel enhancement method, which is able to resolve the drawbacks found in most of the previous Hessian-based methods: 1. eigenvalues are non-uniform throughout an elongated or rounded structure that has uniform intensity; 2. eigenvalues vary with image intensity; and 3. enhancement is not uniform across scales. To address such drawbacks, a modified volume ratio is introduced to ensure method robustness to low magnitude intensity changes in the image. A major issue of this method is the false vessel effect, as also shown in Figure 7j in Section 4.4.3 noise sensitivity.

2.3. Phase Congruency Tensor-based Methods

Many enhancement methods fail due to contrast variations on the image. A significant issue is that they depend on image intensity and, therefore, fine vessels may be missed because of the lower intensity. To address this issue a contrast-independent concept for image features representation, based on Phase Congruency (PC), was introduced in [29].

The development of a contrast-independent vessel enhancement approach, based on the PC concept, has been proposed in [6]. The Phase Congruency Tensor (PCT) combines PC principles with a local tensor representation. This tensor provides a suitable representation of the local image features. Eigenvalues of the PCT tensor can be used, in the same way as Hessian eigenvalues (see Sections 2.2.1 and 2.2.2), to define PCT vesselness and PCT neuriteness measures. An extension of this method into 3D has recently been shown in [30].

A major drawback of the PC-based concept is the complexity of its parameter space. Moreover, as with Hessian-based measures, the PCT-based measures also lead to failure at the intersection of vessels as both eigenvalues have similar, large values leading to PCT-based vesselness and neuriteness measures close to zero.

2.4. Adaptive Histogram Equalisation-based Methods

Contrast Limited Adaptive Histogram Equalisation [10] (CLAHE), originally developed for speculations enhancement in mammograms, is widely used for vessel enhancement. In this simple, histogram-based method an image is first divided into small regions, each of which then undergoes a histogram equalisation. To avoid over-enhancement of noise, a contrast limiting procedure is applied between regions. Further development of this method is demonstrated in [31]and where CLAHE is combined with an anisotropic diffusion filter to smooth the image and preserve vessel boundaries. A major drawback of this method is the noise sensitivity.

2.5. Wavelet Transform-based Enhancement Methods

Bankhead and colleagues [13] propose the use of wavelets for vessel enhancement and segmentation. They calculate an isotropic, undecimated wavelet transform using the cubic B-spline mother wavelet, and employ the coefficients to the threshold steps for enhancement, followed by vessel segmentation. Further improvement of this approach is demonstrated in [32] where multi-orientation and multi-scale features from the vessel filtering and the wavelet transform stages are combined and then used for training the random forest classifier. A major drawback of this method is the complexity of its parameter space.

2.6. Line Detector-based Enhancement Methods

Vessel-like feature enhancement has also been done using multi-scale line detectors [15]. The approach is carried out by changing the length of a primary line detector with the varying scales. The line response, identified by subtraction of average value and the maximum value of each pixel, is computed at 12 different line directions. The main idea behind this method is that line detectors with smaller lengths will avoid the combination of the region of vessel pixels and therefore, provide correct responses. A major drawback of this method is at crossover points, where the method produces 'false vessels' by merging nearby vessels. Further improvement of this method is demonstrated in [33] where a linear combination of all the line responses at varying scales is proposed to produce the final enhancement and segmentation.

2.7. Mathematical Morphology-based Enhancement Methods

Zana and Klein [8] proposed a novel method which combines morphological transforms and cross-curvature evaluation for vessel-like structure enhancement and segmentation. This method relies on the assumption that vessels are linear, connected and have smooth variations of curvature along the peak of the feature as for all curvilinear enhancement methods. First, a sum of top hats is calculated using linear structuring elements with the single size (15-pixels long) at different orientations, and after enhancement step, a curvature measure is calculated using a Laplacian of Gaussian, and finally, both of them are combined to reduce noise and enhance vessel-like structures in an image. Further improvement of this method is demonstrated in [5, 16, 9]. In particular, in [16], an advanced morphological directional filter called path openings is linked with data fusion based on fuzzy set theory. This approach has four steps; First is preprocessing, where the image undergoes histogram equalisation, and then Gaussian filtering to improve the effectiveness of the second step. The second step involves feature extraction by detection of local minima and edges in the image. The third step preserves connected vessels and suppresses noise by path opening, and the final step combines the features and possible paths into a fuzzy classification problem - identifying pixels as likely vessels or likely background.

And most recently, in [9], a multi-scale morphological top hats transform is combined with Gabor and a matched filter. A major issue with this method is that it is quite slow and sensitive to noise.

2.8. Other Approaches

Recently, deep learning approaches have shown great potential for curvilinear structure enhancement and segmentation [34, 35, 36, 37, 38, 39]. In particular, a new regression architecture based on the basis of filter banks learned by sparse convolutional coding is proposed by [38]. The approach is based on a novel initialisation strategy, using carefully designed hand-crafted filters (SCIRD-TS) which are modelling appearance properties of curvilinear structures.

2.9. Limitations and Challenges

Many existing vessel-like structure enhancement methods still have substantial issues when faced with variations in contrast (low-accuracy enhancement), high levels of noise (introduction of 'false vessels' effect), dealing with junctions/bends (suppression of disk-like structures; vessels network connectivity is lost), large image size (high computing time), and complexity of parameter space.

3. Method

In this section, we introduce our novel, mathematical morphology-based method for vessel-like structure enhancement in images: the bowler-hat transform. We highlight the key concepts that allow this method to address the major drawbacks of existing, state-of-the-art, methods.
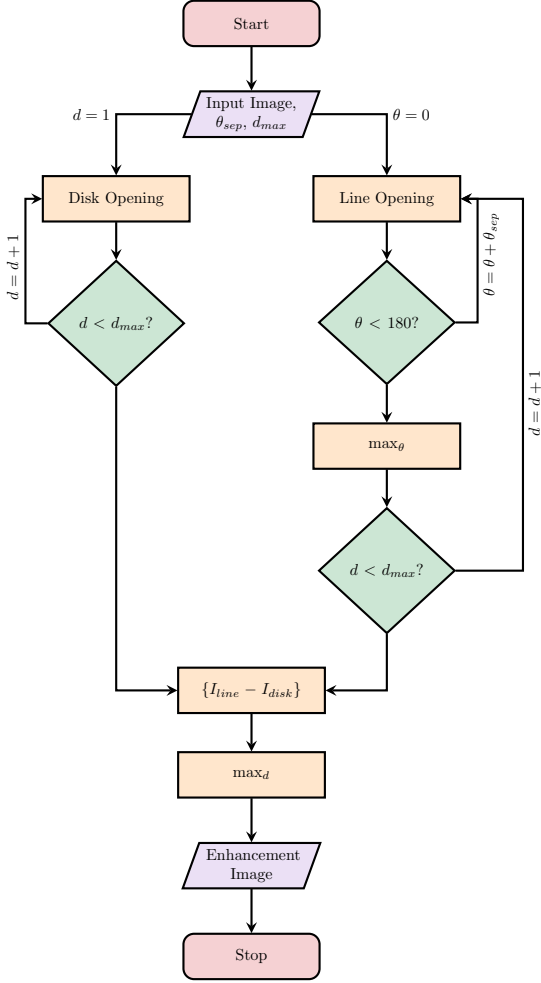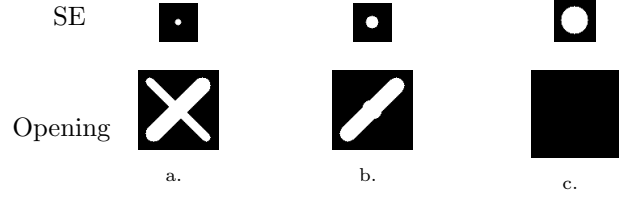
Figure 1: Flow chart of the bowler-hat.

Figure 2: An opening of a simple image with the various size of structuring elements (SE) (the left route in Figure 1). (a) is a result of after a SE smaller than any curvilinear features, (b) is result of after a SE bigger than some curvilinear features but smaller than the other features and (c) is result of after a SE bigger than all curvilinear features in the input image. Reprinted with the permission from [40].
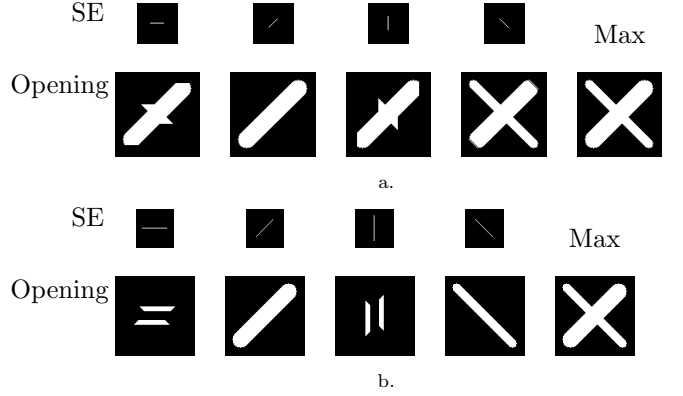

Figure 3: An openings with line SEs of various lengths and rotations of an examplary input image (the right route in Figure 1). (a) is a line SE longer than the width of some curvilinear features in the input image. (b) is a line SE longer than the width of most curvilinear features in the input image. Note how those features aligned with the SE are not attenuated during the opening. In this extremely simple case the maximum (right hand column) includes values at all features. Reprinted with the permission from [40].

3.1. Mathematical Morphology

Morphological operations are a set of non-linear filtering methods formed through a combination of two basic operators: dilation and erosion.

Dilation, ($\oplus$), for a given pixel in a greyscale image, $I(\mathbf{p})$, can be described as the maximum of the points in the weighted neighbourhood described by the structuring element $b(\mathbf{p})$, and mathematically:

$$(I \oplus b)(\mathbf{p}) = \sup_{\mathbf{x} \in E}[I(\mathbf{x}) + b(\mathbf{p} - \mathbf{x})], \qquad (1)$$

where 'sup' is the supremum and $\mathbf{x} \in E$ denotes all points in Euclidean space within the image [41]. Likewise, we mathematically describe the erosion ($\ominus$), as the minimum of the points in the neighbourhood described by the structuring element:

$$(I \ominus b)(\mathbf{p}) = \inf_{\mathbf{x} \in E}[I(\mathbf{x}) + b(\mathbf{p} - \mathbf{x})], \qquad (2)$$

where 'inf' is the infimum [41]. Dilation is able to expand bright areas and reduce dark areas, whilst erosion expands dark areas reducing bright areas as detailed in [42]. From these two operators we can define two commonly used morphological filters:

$$\text{opening}: \quad (I \circ b)(\mathbf{p}) = ((I \ominus b) \oplus b)(\mathbf{p}) \qquad (3)$$
$$\text{closing}: \quad (I \bullet b)(\mathbf{p}) = ((I \oplus b) \ominus b)(\mathbf{p}) \qquad (4)$$

where an opening ($\circ$) will preserve dark features and patterns, suppressing bright features, and a closing ($\bullet$) will preserve bright features whilst suppressing dark patterns.

3.2. Proposed Method

Figure 1 presents a flow diagram of the proposed method which combines the outputs of morphological operations upon an image carried out with two different banks of structural elements: one bank of disk elements with varying radii, and one bank of line elements with varying radii and rotation. The bowler-hat transform is named after the bank of disk elements (forming the bowl) and the bank of line elements (forming the brim). For a given greyscale input image, I, we carry out a series of morphological openings with a bank of disk-shaped structuring elements, b_d of diameter $d \in [1, d_{max}]$ pixels, where d_{max} is the expected maximum vessel size and user-defined parameter.

4

This produces a stack of images, for all d, such that

$$\{I_{disk}\} = \{I \circ b_d : \forall d \in [1, d_{max}]\}. \quad (5)$$

In each I_{disk} image, vessel segments wider than d remain and those segments smaller than d are removed.

We also produce a similar stack of images using a bank of line-shaped structuring elements, $b_{d,\theta}$; each line-shaped is of length $d \in [1, d_{max}]$, with a width of 1 pixel, and orientation $\theta \in [0, 180)$, with the angle step defined by θ_{sep}.

As a result, vessel segments that are longer than d and along the direction defined by θ will remain, and those shorter than d or along the direction defined by θ will be removed. For each line length d we produce a stack of images for all orientations defined by $\theta \in [0, 180)$. Then, for each d, we calculate a single image, I_{line} as a pixel-wise maximum of the stack such that

$$\{I_{line}\} = \{\max_\theta(\{I \circ b_{d,\theta} : \forall \theta\}) : \forall d \in [1, d_{max}]\}. \quad (6)$$

These two stacks, $\{I_{disk}\}$ and $\{I_{line}\}$, are then combined by taking the stack-wise difference, the difference between the maximum opening with a line of length d across all angles and an image formed of opening with a disk of size d, to form the enhanced image. The final enhanced image is then formed from maximum difference at each pixel across all stacks,

$$I_{enhanced} = \max_d(|I_{line} - I_{disk}|). \quad (7)$$

Pixels in the background, *i.e.* dark regions, will have a low value due to the use of openings; pixels in the foreground of blob-like structures will have a low value as the differences will be minimal, *i.e.* similar values for disk-based and line-based openings; and pixels in the foreground of vessel-like structures will have a high value, *i.e.* large differences between longer line-based openings and disk-based openings.

The combination of line and disk elements gives the proposed method a key advantage over the existing methods. Given an appropriate d_{max}, *i.e.* larger than any vessels in the image, a junction should appear bright like those vessels joining that junction, something that many other vessel enhancement methods fail to do. This is due to the ability to fit longer line-based structural elements within the junction area. As a result, the vessels network stays connected when enhanced and segmented, especially at junctions.

In Section 4, we demonstrate, qualitatively and quantitatively, the key advantages of the bowler-hat transform over the existing, state-of-the-art vessel-like structure enhancement methods.

3.3. Implementation and Computation Time

All codes were implemented and written in MATLAB 2016b [43] on Windows 8.1 Pro 64-bit PC running an Intel Core i7-4790 CPU (3.60 GHz) with 16GB RAM. The
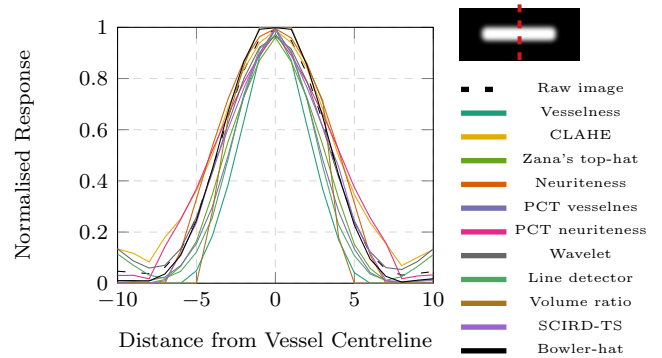

Figure 4: Cross-sectional profiles of a synthetic vessel input image (at the up right side (red, dashed line)) and the input image enhanced with the state-of-the-art (see legend for colours) vessel enhancement methods and the proposed bowler-hat (black, solid line) vessel enhancement method. All the images were normalised such that the brightest pixel in the whole image has a value of 1 and the darkest a value of 0.

source code is available in a GitHub repository https://github.com/CigdemSazak/bowler-hat-2d.

The average computation time for the proposed method is 3.8 seconds for DRIVE image and 4.9 seconds for STARE image. Please make a note that the proposed method has been implemented and tested in Matlab, however, C++ implementation could be much faster.

4. Results

In this section, the proposed method is qualitatively and quantitatively validated and compared with the existing state-of-the-art methods using synthetic and clinically relevant, retinal image datasets, with human-annotated ground truths, and other biomedical images.

As with any image processing method, an understanding of how the parameters involved affect the result is essential. In general, we have found the bowler-hat transform to be robust, usually requiring 10–12 θ orientations for line structuring element and the size of the disk/line structuring element d to be greater than the thickest vessel structure in an image.

The following sections are organised as follows: first, we visually and qualitatively analyse the bowler-hat transform and compare with alternative methods in Section 4.1, Section 4.3, Section 4.2. Second, we use real world fundus images, with human-created ground truths, to compare these methods in Section 4.4 and the parameters for the all methods can be found in the supplementary file presented in Table 1. We evaluate these results in a quantitative and comparable manner using the Receiver Operating Characteristic (ROC) curve and the Area Under the Curve (AUC) metric. All the images were normalised after each enhancement approach such that the brightest pixel in the whole image has a value of 1 and the darkest a value of 0.

4.1. Profile Analysis

The effect of the vessel enhancement methods on a simple vessel-like structure is shown in Figure 4. This represents the simplest example of a vessel in an image, like those found in retinal images. Figure 4 illustrates the normalised, intensity profile for images enhanced with each of the methods. As the Figure 4 clearly shows, the enhancement methods tend to expand or shrink the vessel-like structures. Moreover, while the Hessian-based methods have an enhanced signal at the center of the vessel, *i.e.* a peak value of one at the vessels centre-line, their value quickly drops off and decreases the perceived thickness of the vessel. The proposed method has both these benefits: a maximal peak value at the vessel centre-line and an enhanced response to the edges of the vessel. As a result, reliable vessel thickness can be captured.

4.2. Response to Uneven Background Illumination

Figure 5 presents the response of the proposed method to an uneven illumination scenario. Key features such as junctions are preserved and appear unaffected by even severe illumination problems. This ability to preserve junctions under uneven illumination is important for many real applications of vessel enhancement and the proposed method is able to do this, unlike the current state-of-the-art methods.
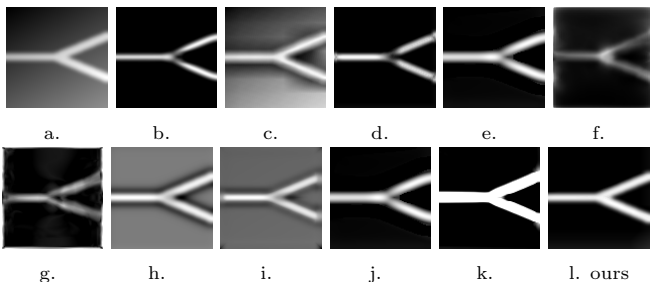

Figure 5: Comparison of the vessel enhancement methods' abilities to deal with an uneven background illumination. (a) an input image, (b) vesselness, (c) CLAHE, (d) Zana's top-hat, (e) neuriteness, (f) PCT vesselness, (g) PCT neuriteness, (h) wavelet, (i) line detector, (j) volume ratio, (k) SCIRD-TS, and (l) the bowler-hat.

4.3. Response to Vessels, Intersections, and Blobs

Figure 6 presents a qualitative comparison between the proposed method and the state-of-the-art methods when applied to synthetic images and real images with vessel-like, intersection-like, and blob-like structures. Key issues that occur across the state-of-the-art methods include defects at junctions (purple arrows), noise enhancement, tip artefacts (orange arrows) and loss of signal (yellow arrows). These issues are all absent with our proposed method. However, a shortcoming of our approach is shown in Figure 6- row 4, which shows a vessel like an object with an attached 'blob' (green arrow), a perfect vessel enhancement method would enhance all of the linear structure and none of the blob. While none of the compared approaches act in this ideal manner, many of the methods show a clear difference between the blob response and vessel response.

4.4. Real Data - Retinal Image Datasets

In this section, we show the quality of the proposed method validated on three publicly available retinal image datasets: the DRIVE, STARE, and HRF databases. These datasets have been chosen because of their availability and their ground truth data. We have used these ground truth segmentations to quantitatively compare the proposed method with the other vessel enhancement methods.

The Digital Retinal Images for Vessel Extraction [44] (DRIVE) dataset is a published database of retinal images for research and educational purposes. The database consists of twenty colour images that are JPEG compressed, as for many screening programs. These images were selected randomly from a screening of 400 diabetic subjects between the ages of 25 and 90. The ground truth provided with this dataset consists of manual segmentation of the vasculature for each image. Ground truths were prepared by trained observers, and 'true' pixels are those for which observers where > 70% certain.

The STructured Analysis of the REtina (STARE) [45] dataset is another publicly available database containing twenty colour images with human-determined vasculature ground truth. We have compared all these images against the AH labelling. The High-Resolution Fundus (HRF) image dataset [46] consists of 45 retinal images. This dataset has three type of subjects include healthy, diabetic retinopathy, and glaucoma.

4.4.1. Quantitative Validation - Enhancement

While a visual inspection can give some information regarding the effectiveness of the vessel enhancement methods, a form of quantitative validation is required. Therefore, as proposed in [47], we have used the Receiver Operating Characteristic (ROC) curve and we calculated the Area Under the Curve (AUC) based on ROC curve to compare the vessel enhancement methods. To derive the ROC curve and then to calculate the AUC value, each enhanced image is segmented at different thresholds ranging from 0 to 1, andcompared with the corresponding ground truth segmentation [43]. AUC value is calculated using trapezoidal approximation of the area under the curve. The AUC metric measures vessel segmentation accuracy directly but it also measures the vessel enhanced accuracy indirectly. Such a procedure is used for Figure 11, Figure 8, and Table 1.

Please note that, before any quantitative evaluation, all the enhanced retinal images were masked with the mask images provided with the retinal image datasets.

4.4.2. Quantitative Validation - Segmentation

To quantitatively evaluate the robustness of the vessel segmentation methods, sensitivity (SE), specificity (SP), and accuracy (ACC) metrics are calculated for each segmented image and its corresponding ground truth segmentation, as follows:
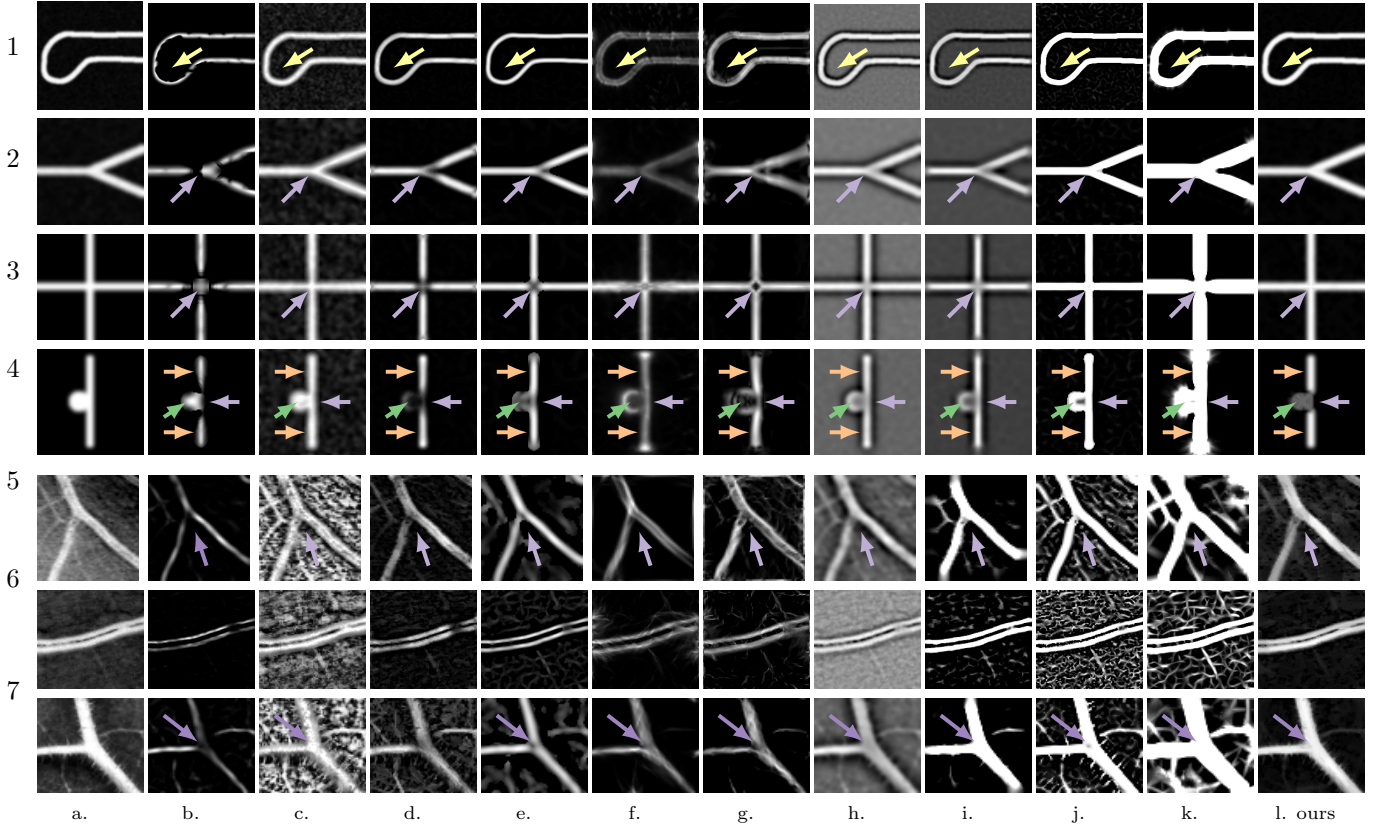
Figure 6: The bowler-hat transform enhances vessels, maintaining junctions and tips while suppressing blobs. A comparison of the enhancement of vessel-like and other structures using the proposed method and the state-of-the-art methods. (a) shows the original images, all vessels have a thickness of 9 pixels and the 'blob' in 4 has a diameter of 21 pixels. The first four rows are synthetic images that indicate possible vessel-like structures in biomedical images. The last three rows illustrate vessel-like structures from real biomedical images. Row 5 is a cropped region from the DRIVE dataset, while row 6 is vessel section of the healthy images in the HRF dataset. The last row is another a cropped region from the leaf image [6]. Results for (b) vesselness, (c) CLAHE, (d) Zana's top-hat, (e) neuriteness, (f) PCT vesselness, (g) PCT neuriteness, (h) wavelet, (i) line detector, (j) volume ratio, (k) SCIRD-TS, and (l) the bowler-hat. Arrows indicate features of interest: vessel structures (yellow arrows), junctions (purple), blob-like features (green), and tips (orange).

$$SE = \frac{TP}{TP + FN}, \tag{8}$$

$$SP = \frac{TN}{TN + FP}, \tag{9}$$

$$ACC = \frac{TP + TN}{TP + TN + FP + FN}, \tag{10}$$

where TP is the true positive count, FP the false positive count, TN the true negative and FN the false negative counts of the segmented pixels. We used these metrics in Table 2 and Table 3.

4.4.3. Healthy Subjects

Figure 7 shows the results of the proposed and state-of-the-art methods applied to a sample image from the HRF dataset (results for DRIVE and STARE datasets can be found in Supplementary Materials).

We can see that the proposed method is able to enhance finer structures as detected by the human observer but not emphasised by many of the other methods (see arrows).

We can also see that, whilst the connectivity seems to be maintained (unlike in Figure 7b), 'false vessels' are not introduced (c.f. Figure 7e).

Finally, Figure 8 and Table 1 present ROC curves and mean AUC values for the enhancement results of the proposed and state-of-the-art methods applied to all images across the DRIVE, STARE and HRF datasets by using the quantitative validation as described Section 4.4.1.

4.4.4. Unhealthy Subjects

Figure 9 presents a visual comparison of the enhancement methods applied to sample images of subjects with diabetic retinopathy and with glaucoma from the DRIVE, STARE and HRF datasets. As we can notice in Figure 9i, the proposed method is sensitive to noisy regions. This issue can be addressed by the use of a line-shaped morphological structuring element with a varying thickness. Even so, the proposed method achieved a highest overall score on the HRF unhealthy images as illustrated in Table 1

4.4.5. Enhancement with Global and Local Thresholding

Figure 10 demonstrates the vessel segmentation results obtained by the proposed and the state-of-the-art
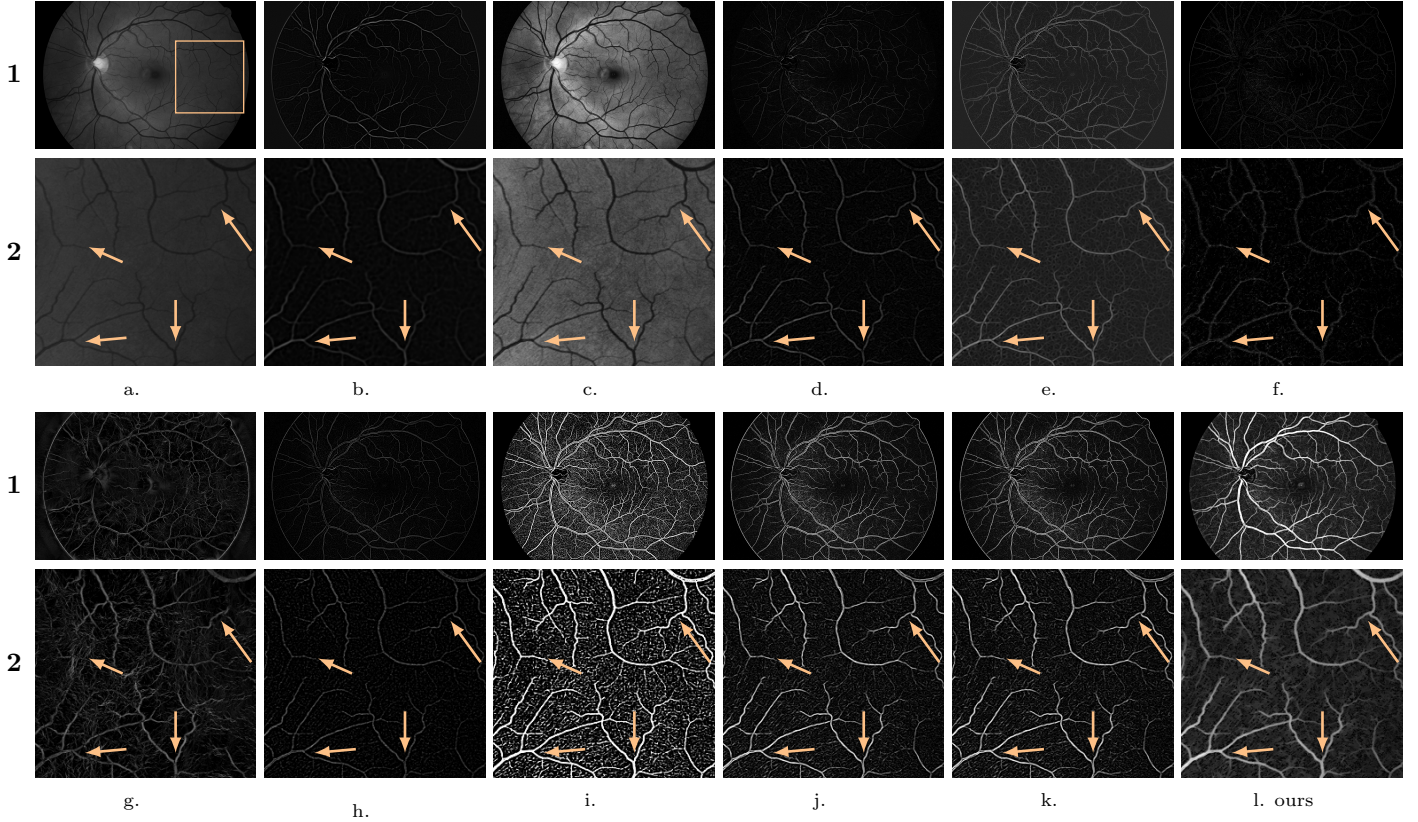
Figure 7: A comparison of the vessel-like structure enhancement results for a sample image from HRF dataset. (a) an input image. The zoomed in region (2) shows enlarged image ROI in the square of the raw image. The arrows point to key areas of interest, such as junctions, fine tips and vessels not captured by all methods. Respectively, (b) vesselness, (c) CLAHE, (d) Zana's top-hat, (e) neuriteness, (f) PCT vesselness, (g) PCT neuriteness, (h) wavelet, (i) line detector, (j) volume ratio, (k) SCIRD-TS, and (l) the bowler-hat.
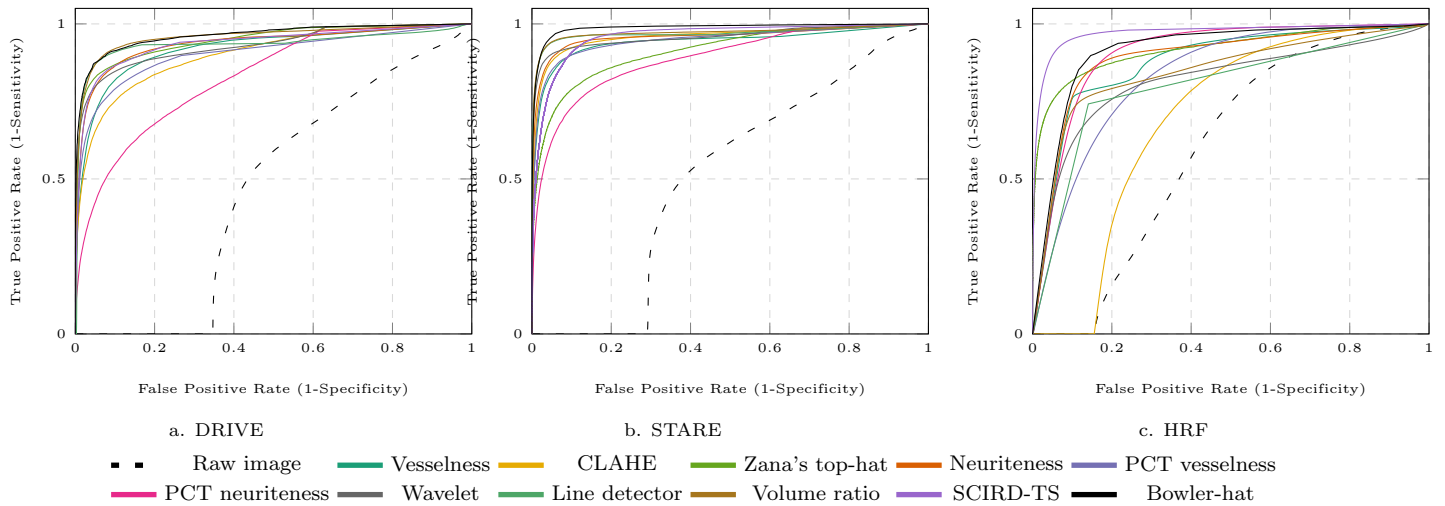

Figure 8: ROC curves calculated for sample images from the (a) DRIVE, (b) STARE, and (c) HRF datasets enhanced by the proposed and the state-of-the-art methods (see legend for colours). Corresponding mean AUC values can be found in Table 1.

vessel-like structures enhancement methods followed by the same global and local thresholding approaches proposed in [48, 49] when applied to the HRF dataset images. The quantitative comparision of the vessel segmentation results obtained is presented in Table 2.

4.4.6. Comparison with Other Segmentation Methods

To highlight the effectiveness of the proposed vessel enhancement method (combined with the local thresholding approach [49]) for a full vessel segmentation, we compared the performance of our method with seventeen state-of-the-art vessel segmentation methods reported in the liter-

Enhancement Method		AUC (StDev)			
	Year/Ref	DRIVE	STARE	HRF(healthy)	HRF(unhealthy)
Raw image	-	0.416 (0.064)	0.490 (0.076)	0.530 (0.075)	0.541(0.073)
Vesselness	1998 [3]	0.888 (0.243)	0.898 (0.215)	0.913 (0.020)	0.904 (0.020)
CLAHE	1998 [10]	0.862 (0.068)	0.880 (0.087)	0.867 (0.025)	0.835 (0.023)
Zana's top-hat	2001 [8]	0.933 (0.015)	0.956 (0.021)	0.943 (0.010)	0.91 (0.016)
Neuriteness	2004 [26]	0.909 (0.022)	0.927 (0.039)	0.896 (0.024)	0.879 (0.059)
PCT vesselness	2012 [6]	0.890 (0.037)	0.899 (0.056)	0.888 (0.011)	0.837 (0.030)
PCT neuriteness	2012 [6]	0.817 (0.121)	0.827 (0.165)	0.901 (0.029)	0.777 (0.022)
Wavelet	2012 [13]	0.891 (0.024)	0.867 (0.042)	0.802 (0.022)	0.740 (0.026)
Line detector	2013 [15]	0.828 (0.024)	0.856 (0.042)	0.820 (0.022)	0.734 (0.026)
Volume ratio	2016 [28]	0.934 (0.024)	0.939 (0.042)	0.926 (0.022)	0.823 (0.026)
SCIRD-TS	2016 [38]	0.925 (0.468)	0.946 (0.021)	0.956 (0.012)	0.0692 (0.035)
Bowler-hat	-	**0.946 (0.032)**	**0.962 (0.034)**	**0.968 (0.015)**	**0.944 (0.016)**

Table 1: Mean AUC values calculated as described in Section 4.4.1, for the images across the DRIVE, STARE and HRF datasets enhanced by the bowler-hat and the state-of-the-art methods. Best results for each dataset are in bold. Individual ROC curves can be seen in Figure 8.

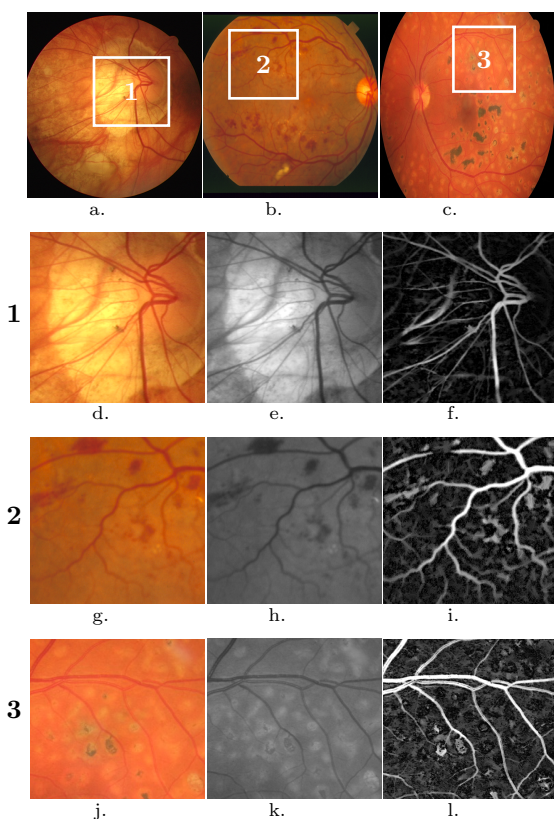ature [44, 50, 51, 52, 53, 54, 55, 56, 57, 58, 12, 15, 13, 59,

Figure 9: The bowler-hat applied to the unhealthy subjects from (a) DRIVE, (b) STARE and (c) HRF. (d, g, j) are the input images with the region of interest. (e, h, k) illustrate the green channel of input image (f, i, l) demonstrate the enhancement result of the vessel-like structure on the abnormal area.

Enhancement Method		ACC (Std)	
		Global	Local
	Year/Ref	HRF	HRF
Vesselness	1998 [3]	0.936(0.006)	0.951(0.006)
CLAHE	1998 [10]	0.668(0.101)	0.859(0.009)
Zana's top-hat	2001 [8]	0.925(0.016)	0.946(0.008)
Neuriteness	2004 [26]	0.948(0.005)	0.953(0.006)
PCT vesselness	2012 [6]	0.892(0.015)	0.926(0.007)
PCT neuriteness	2012 [6]	0.916(0.013)	0.900(0.008)
Wavelet	2012 [13]	0.672(0.137)	0.946(0.006)
Line detector	2013 [15]	0.902(0.008)	0.957(0.006)
Volume ratio	2016 [28]	0.936(0.012)	0.947(0.011)
SCIRD-TS	2016 [38]	0.947(0.008)	0.951(0.010)
Bowler-hat	-	**0.960(0.005)**	**0.961(0.005)**

Table 2: Mean ACC values with the standard deviation for vessel segmentation results obtained by the proposed and the state-of-the-art vessel-like structures enhancement methods followed by the same global thresholding approach proposed in [48] and local thresholding approach proposed in [49] when applied to the HRF dataset images.

60, 61, 46] applied to DRIVE, STARE and HRF datasets.

Table 3 shows the reported results of the seventeen segmentation methods compared with the proposed method. From Table 3, it can be seen that the proposed bowler-hat transform outperforms several common or state-of-the-art methods from the field. In cases where the proposed method does not outperform, but still performs to a similar quality, it is worth keeping in mind that many of these methods combine multiple stages, of which enhancement is
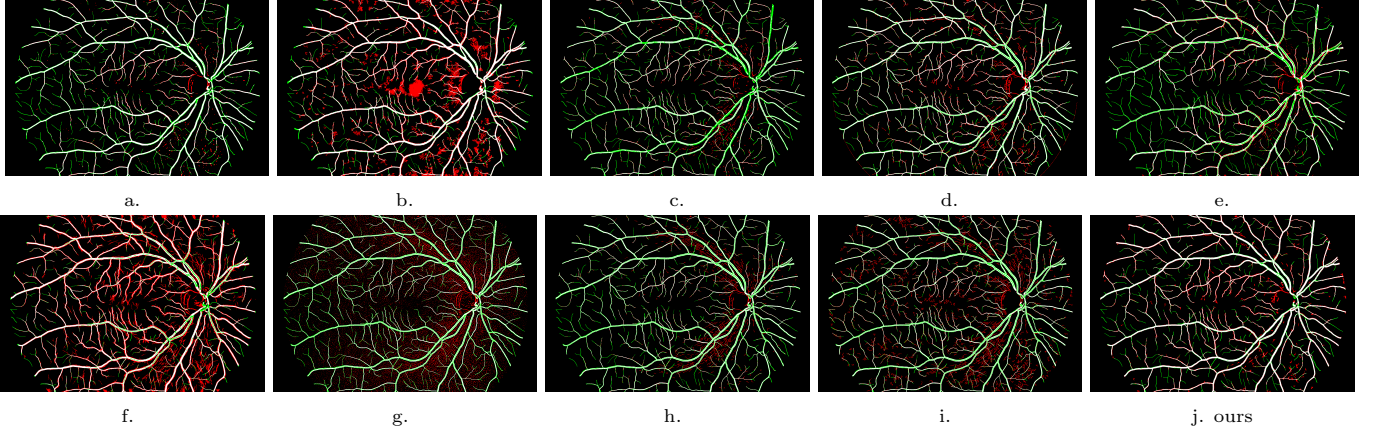
Figure 10: Vessel segmentation results obtained by the proposed and the state-of-the-art vessel-like structures enhancement methods followed by the same local thresholding approach proposed in [49] when applied to the HRF dataset images. (a) vesselness, (b) CLAHE, (c) Zana's top-hat, (d) neuriteness, (e) PCT vesselness, (f) PCT neuriteness, (g) wavelet, (h) line detector, (i) volume ratio, and (j) the bowler-hat. Colours indicate true positive (white), false positive (red) and false negative pixels (green). Corresponding mean AUC values can be found in Table 2.

Method	DRIVE			STARE			HRF		
	SE	SP	ACC	SE	SP	ACC	SE	SP	ACC
Staal et.al [44]	-	-	0.946	-	-	0.951	-	-	-
Soares et.al [50]	-	-	0.946	-	-	0.948	-	-	-
Lupascu et.al [51]	0.720	-	**0.959**	-	-	-	-	-	-
You et.al [52]	0.741	0.975	0.943	0.726	0.975	0.949	-	-	-
Marin et.al [53]	0.706	0.980	0.945	0.694	0.981	0.952	-	-	-
Wang et.al [54]	-	-	0.946	-	-	0.952	-	-	-
Mendonca et.al [55]	0.734	0.976	0.945	0.699	0.973	0.944	-	-	-
Palomera-Perez et.al [56]	0.660	0.961	0.922	**0.779**	0.940	0.924	-	-	-
Matinez-Perez et.al [57]	0.724	0.965	0.934	0.750	0.956	0.941	-	-	-
Al-Diri et.al [58]	0.728	0.955	-	0.752	0.968	-	-	-	-
Fraz et.al [12]	0.715	0.976	0.943	0.731	0.968	0.944	-	-	-
Nguyen et.al [15]	-	-	0.940	-	-	0.932	-	-	-
Bankhead et.al [13]	0.703	0.971	0.937	0.758	0.950	0.932	-	-	-
Orlando et.al [59]	**0.785**	0.967	-	-	-	-	-	-	-
Azzopardi et.al [60]	0.766	0.970	0.944	0.772	0.970	0.950	-	-	-
Odstrcilik et.al [46]	0.784	0.951	0.934	0.706	0.969	0.934	0.786	0.975	0.953
Zhang et.al [61]	0.774	0.972	0.947	0.779	0.975	0.955	0.797	0.971	0.955
Proposed method	0.718	**0.981**	**0.959**	0.730	**0.979**	**0.962**	**0.831**	**0.981**	**0.963**

Table 3: Performance of different vessel segmentation methods have been reported in the literature with the proposed method, regarding mean sensitivity (SE), specificity (SP), accuracy (ACC) on the all over the DRIVE, STARE and HRF datasets.

just one, whereas our approach is able to achieve such high quality results with just an enhancement process. The results on both datasets demonstrate that the sensitivity of the proposed method is not in top three respectively for DRIVE ($SE = 0.616$) and STARE ($SE = 0.730$). However, the proposed method has the highest score with the specificity ($SP = 0.991$) for DRIVE and ($SP = 0.979$) for STARE. Most importantly, our method has the accuracy ($ACC = 0.960$) and ($ACC = 0.962$) for DRIVE and STARE respectively; the highest compared to other vessel segmentation methods. Finally, the proposed method has the highest score for HRF dataset, with ($SE = 0.831$), ($SP = 0.981$) and ($ACC = 0.963$).

4.5. Response to Noise

To test how the state-of-the-art enhancement methods and the proposed method behave with the different level and type of the noise, a noisy synthetic image that includes a single vessel-like structure was used. We generated such noisy image by optimising the noise generation parameters to achieve a target PSNR by using a genetic optimisation algorithm proposed in [62].

We then examine the enhancement methods by increasing the noise level and then calculating the AUC values for each level of noise and each comparator method. Figure 11 shows the effect of three different noise types on the proposed and state-of-the-art methods. Given that the pro-
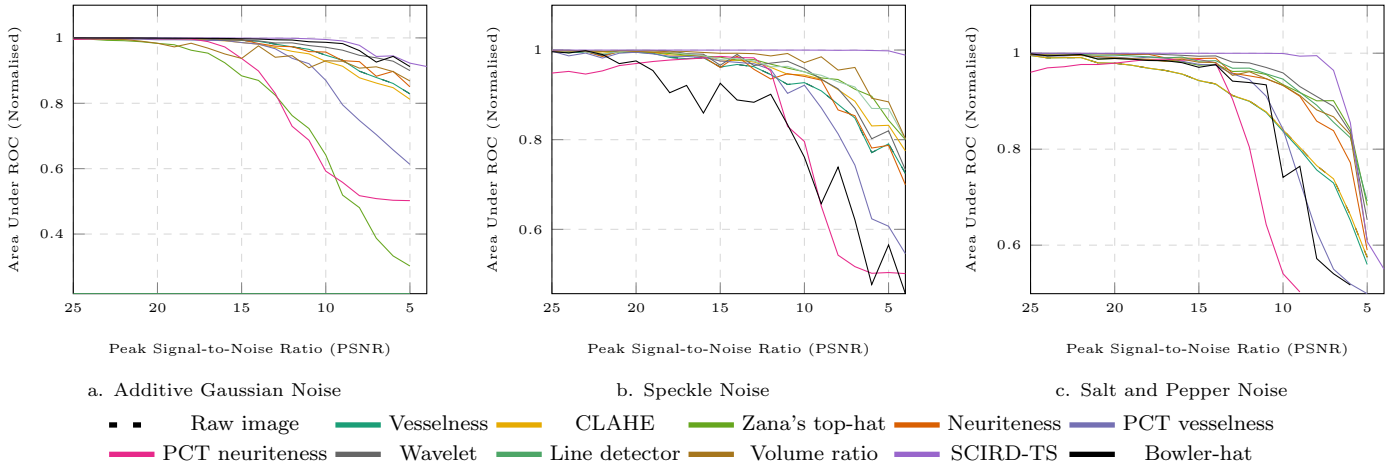
Figure 11: The bowler-hat transform is robust against additive Gaussian noise but susceptible to speckle and salt&pepper. Mean AUC for the input image and the image enhanced by bowler-hat and by the state-of-the-art methods with different peak signal-to-noise ratios (PSNRs) for three different noise types: (a) additive Gaussian noise, (b) multiplicative Gaussian noise, and (c) salt and pepper noise (see legend for colours).

posed method has no built-in noise suppression, it is unsurprising that the effect of noise on the enhanced image is in-line with the raw image. We note that the method is weakest in response to speckle noise (multiplicative Gaussian) and also weak in response to salt and pepper noise. This follows from the noise-sensitivity in morphological operations and should be taken into consideration when choosing an enhancement method.

4.6. Other Biomedical Data

While we have demonstrated the proposed method on the enhancement of vessel-like structures, the approach is feasible for a wide range of biomedical images, see Figure 12.

5. Conclusion and Discussion

A wide range of image processing methods have been proposed for vessel-like structure enhancement in biomedical images, see section Section 1. Most of them, however, suffer from issues with low-contrast signals, enhancement of noise or when dealing with junctions.

In this paper, we introduce a new enhancement method for vessel-like structures based on mathematical morphology, which exploits the elongated shape of vessel-like structures. The proposed method, the bowler-hat transform, was qualitatively and quantitatively validated and compared with the state-of-the-art methods using a range of synthetic and real image datasets, including retinal image collections (DRIVE, STARE and HRF). We showed the effectiveness of the bowler-hat transform, and its superior performance on retinal imaging data, see Figure 8, Table 1, and Table 2. Furthermore, experimental results on the unhealthy retinal images have shown that the vessels enhanced by our bowler hat transform are continuous and complete in problematic regions as illustrated in Figure 9.

As with any image processing technique, our proposed method has limitations. Basically, morphological operations are renowned for their large computational requirements. Another limitation of the proposed method is displayed in Figure 6 row 4, which shows a vessel-like structure with an attached 'blob' (green arrow), a perfect vessel enhancement method would enhance all of the linear structure and none of the blob. Whilst none of the comparison methods act in this ideal manner many of them show a clear difference between the blob response and vessel response, our proposed method shows some difference, but this difference impacts the signal of the vessel.

Moreover, as we note in Figure 7, the proposed method is sensitive to noise such as susceptible to speckle and salt&pepper, as is the PCT neuriteness method in Figure 7g. In the future, we will investigate introducing a line-shaped morphological structuring element with varying thickness to address this issue. Nevertheless, our implementation demonstrates an improved and easy to use vessel enhancement alternative that can be used in a wide range of biomedical imaging scenarios [63]. Whilst one would expect the lack of noise suppression to be a major issue with regard to quantified measurements of vessel enhancement, we find that the proposed method gives the best enhancement of all methods on the DRIVE, STARE and HRF datasets (see Table 1 and Figure 8).

In this paper, we have demonstrated the ability of the proposed bowler-hat transform to effectively enhance and segment vessel-like structures in the retinal images. In addition, to illustrate the robustness of the proposed bowler-hat transform enhance, we have matched it with the seventeen state-of-the-art methods previously tested on the DRIVE, STARE and HRF image datasets, see Table 3.

Future extensions of this work will include the development of a three-dimensional equivalent, exploration of blob-like structures enhancing variants of this method, and an analysis of parameter sensitivity for different modali-
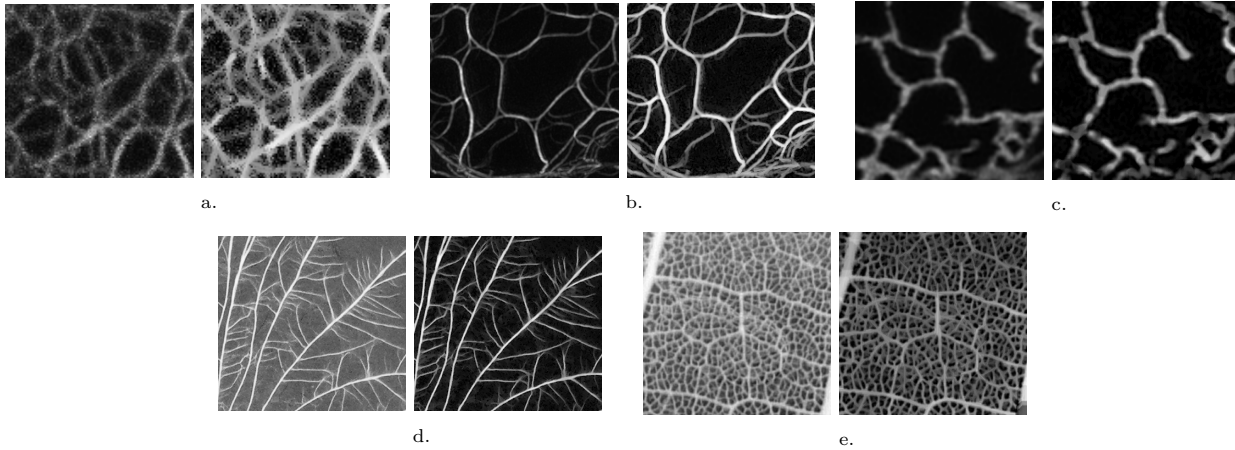
11

Figure 12: Results of the vessel-like structure enhancement using the bowler-hat on biological images of (a–b) cytoskeletal networks, (c) endoplasmic reticulum, and (d–e) macro-scale networks . (a) provided by Prof. R. Leube, RWTH Aachen University, Germany. (b) provided by Dr T. Hawkins, Durham University, UK. (c–e) provided by Prof. M. Fricker, Oxford University, UK.

ties.

References

[1] P. Bibiloni, M. Gonzalez-Hidalgo, S. Massanet, A survey on curvilinear object segmentation in multiple applications, Pattern Recognition 60 (C) (2016) 949–970.

[2] M. Fraz, P. Remagnino, A. Hoppe, B. Uyyanonvara, A. Rudnicka, C. Owen, S. Barman, Blood vessel segmentation methodologies in retinal images a survey, Computer Methods and Programs in Biomedicine 108 (1) (2012) 407 – 433.

[3] A. F. Frangi, W. J. Niessen, K. L. Vincken, M. A. Viergever, Multiscale vessel enhancement filtering, in: International Conference on Medical Image Computing and Computer-Assisted Intervention, Springer, 1998, pp. 130–137.

[4] R. Su, C. Sun, T. D. Pham, Junction detection for linear structures based on hessian, correlation and shape information, Pattern Recognition 45 (10) (2012) 3695–3706.

[5] R. Su, C. Sun, C. Zhang, T. D. Pham, A new method for linear feature and junction enhancement in 2D images based on morphological operation, oriented anisotropic Gaussian function and Hessian information, Pattern Recognition 47 (10) (2014) 3193–3208.

[6] B. Obara, M. Fricker, D. Gavaghan, V. Grau, Contrast-independent curvilinear structure detection in biomedical images, IEEE Transactions on Image Processing 21 (5) (2012) 2572–2581.

[7] B. Obara, M. Fricker, V. Grau, Coherence enhancing diffusion filtering based on the phase congruency tensor, in: IEEE International Symposium on Biomedical Imaging, 2012, pp. 202–205.

[8] F. Zana, J. C. Klein, Segmentation of vessel-like patterns using mathematical morphology and curvature evaluation, IEEE Transactions on Image Processing 10 (7) (2001) 1010–1019.

[9] C.-Y. Lu, B.-Z. Jing, P. P. Chan, D. Xiang, W. Xie, J. Wang, D. S. Yeung, Vessel enhancement of low quality fundus image using mathematical morphology and combination of gabor and matched filter, in: International Conference on Wavelet Analysis and Pattern Recognition, 2016, pp. 168–173.

[10] E. D. Pisano, S. Zong, B. M. Hemminger, M. DeLuca, R. E. Johnston, K. Muller, M. P. Braeuning, S. M. Pizer, Contrast limited adaptive histogram equalization image processing to improve the detection of simulated speculations in dense mammograms, Journal of Digital Imaging 11 (4) (1998) 193–200.

[11] P. Feng, Y. Pan, B. Wei, W. Jin, D. Mi, Enhancing retinal image by the Contourlet transform, Pattern Recognition 28 (4) (2007) 516–522.

[12] M. Fraz, S. Barman, P. Remagnino, A. Hoppe, A. Basit, B. Uyyanonvara, A. Rudnicka, C. Owen, An approach to localize the retinal blood vessels using bit planes and centerline detection, Computer Methods and Programs in Biomedicine 108 (2) (2012) 600 – 616.

[13] P. Bankhead, C. N. Scholfield, J. G. McGeown, T. M. Curtis, Fast retinal vessel detection and measurement using wavelets and edge location refinement, PloS One 7 (3) (2012) e32435.

[14] G. Azzopardi, N. Petkov, Automatic detection of vascular bifurcations in segmented retinal images using trainable COSFIRE filters, Pattern Recognition Letters 34 (8) (2013) 922–933.

[15] U. T. Nguyen, A. Bhuiyan, L. A. Park, K. Ramamohanarao, An effective retinal blood vessel segmentation method using multiscale line detection, Pattern Recognition 46 (3) (2013) 703–715.

[16] E. M. Sigurosson, S. Valero, J. A. Benediktsson, J. Chanussot, H. Talbot, E. Stefansson, Automatic retinal vessel extraction based on directional mathematical morphology and fuzzy classification, Pattern Recognition Letters 47 (C) (2014) 164–171.

[17] B. Chen, Y. Chen, Z. Shao, L. Luo, Retinal vessel enhancement using multi-dictionary and sparse coding, in: IEEE International Conference on Acoustics, Speech and Signal Processing, 2016, pp. 893–897.

[18] O. Merveille, H. Talbot, L. Najman, N. Passat, Curvilinear structure analysis by ranking the orientation responses of path operators, IEEE Transactions on Pattern Analysis and Machine Intelligence 40 (2) (2018) 304–317.

[19] M. Tabb, N. Ahuja, Multiscale image segmentation by integrated edge and region detection, IEEE Transactions on image processing 6 (5) (1997) 642–655.

[20] J. Weickert, Anisotropic diffusion in image processing, Vol. 1, 1998.

[21] P. Perona, J. Malik, Scale-space and edge detection using anisotropic diffusion, IEEE Transactions on pattern analysis and machine intelligence 12 (7) (1990) 629–639.

[22] S. Zheng, A. Yuille, Z. Tu, Detecting object boundaries using low-, mid-, and high-level information, Computer Vision and Image Understanding 114 (10) (2010) 1055–1067.

[23] J. Canny, A computational approach to edge detection, in: Readings in Computer Vision, Elsevier, 1987, pp. 184–203.

[24] M. S. Rebelo, S. S. Furuie, M. A. Gutierrez, E. Costa, L. Moura, Multiscale representation for automatic identification of structures in medical images, Computers in Biology and Medicine 37 (8) (2007) 1183–1193.

[25] K. Krissian, J. Ellsmere, K. Vosburgh, R. Kikinis, C.-E. Westin, Multiscale segmentation of the aorta in 3D ultrasound images, in: IEEE International Conference of the Engineering in Medicine and Biology Society, Vol. 1, 2003, pp. 638–641.

[26] E. Meijering, M. Jacob, J.-C. Sarria, P. Steiner, H. Hirling, M. Unser, Design and validation of a tool for neurite tracing and analysis in fluorescence microscopy images, Cytometry Part A 58A (2) (2004) 167–176.

[27] T. Smafield, V. Pasupuleti, K. Sharma, R. L. Huganir, B. Ye, J. Zhou, Automatic dendritic length quantification for high throughput screening of mature neurons, Neuroinformatics 13 (4) (2015) 443–458.

[28] T. Jerman, F. Pernuš, B. Likar, Ž Špiclin, Enhancement of vascular structures in 3D and 2D angiographic images, IEEE Transactions on Medical Imaging 35 (9) (2016) 2107–2118.

[29] P. Kovesi, Phase congruency detects corners and edges, in: The Australian Pattern Recognition Society Conference, 2003, pp. 309–318.

[30] C. Sazak, B. Obara, Contrast-independent curvilinear structure enhancement in 3D biomedical images, in: IEEE International Symposium on Biomedical Imaging, Melbourne, Australia, 2017, pp. 1165–1168.

[31] Y. Q. Zhao, X. H. Wang, X. F. Wang, F. Y. Shih, Retinal vessels segmentation based on level set and region growing, Pattern Recognition 47 (7) (2014) 2437–2446.

[32] J. Zhang, Y. Chen, E. Bekkers, M. Wang, B. Dashtbozorg, B. M. ter Haar Romeny, Retinal vessel delineation using a brain-inspired wavelet transform and random forest, Pattern Recognition 69 (C) (2017) 107–123.

[33] Y. Hou, Automatic segmentation of retinal blood vessels based on improved multiscale line detection, Journal of Computing Science and Engineering 8 (2) (2014) 119–128.

[34] M. W. Law, A. C. Chung, Efficient implementation for spherical flux computation and its application to vascular segmentation, IEEE Transactions on Image Processing 18 (3) (2009) 596–612.

[35] R. Rigamonti, V. Lepetit, Accurate and efficient linear structure segmentation by leveraging ad hoc features with learned filters, in: International Conference on Medical Image Computing and Computer-Assisted Intervention, 2012, pp. 189–197.

[36] B. S. Lam, Y. Gao, A. W.-C. Liew, General retinal vessel segmentation using regularization-based multiconcavity modeling, IEEE Transactions on Medical Imaging 29 (7) (2010) 1369–1381.

[37] R. Annunziata, A. Kheirkhah, P. Hamrah, E. Trucco, Boosting hand-crafted features for curvilinear structure segmentation by learning context filters, in: International Conference on Medical Image Computing and Computer-Assisted Intervention, 2015, pp. 596–603.

[38] R. Annunziata, E. Trucco, Accelerating convolutional sparse coding for curvilinear structures segmentation by refining scird-ts filter banks, IEEE Transactions on Medical Imaging 35 (11) (2016) 2381–2392.

[39] E. Grisan, Boosted learned kernels for data-driven vesselness measure, in: Medical Imaging 2017: Biomedical Applications in Molecular, Structural, and Functional Imaging, Vol. 10137, 2017, p. 101370Z.

[40] C. NELSON, Mathematical morphology for quantification in biological & medical image analysis, Ph.D. thesis, Durham University (2017).

[41] N. Efford, Digital image processing: a practical introduction using java (with CD-ROM), Addison-Wesley Longman Publishing Co., Inc., 2000.

[42] R. M. Haralick, S. R. Sternberg, X. Zhuang, Image analysis using mathematical morphology, IEEE Transactions on Pattern Analysis and Machine Intelligence (4) (1987) 532–550.

[43] I. The Mathworks, Matlab, www.mathworks.com (2016).

[44] J. Staal, M. Abramoff, M. Niemeijer, M. Viergever, B. van Ginneken, Ridge based vessel segmentation in color images of the retina, IEEE Transactions on Medical Imaging 23 (4) (2004) 501–509.

[45] A. D. Hoover, V. Kouznetsova, M. Goldbaum, Locating blood vessels in retinal images by piecewise threshold probing of a matched filter response, IEEE Transactions on Medical Imaging 19 (3) (2000) 203–210.

[46] J. Odstrcilik, R. Kolar, A. Budai, J. Hornegger, J. Jan, J. Gazarek, T. Kubena, P. Cernosek, O. Svoboda, E. Angelopoulou, Retinal vessel segmentation by improved matched filtering: evaluation on a new high-resolution fundus image database, IET Image Processing 7 (4) (2013) 373–383.

[47] T. Fawcett, An introduction to roc analysis, Pattern Recognition Letters 27 (8) (2006) 861–874.

[48] N. Otsu, A threshold selection method from gray-level histograms, IEEE Transactions on Systems, Man, and Cybernetics 9 (1) (1979) 62–66.

[49] X. Jiang, D. Mojon, Adaptive local thresholding by verification-based multithreshold probing with application to vessel detection in retinal images, IEEE Transactions on Pattern Analysis and Machine Intelligence 25 (1) (2003) 131–137.

[50] J. V. Soares, J. J. Leandro, R. M. Cesar, H. F. Jelinek, M. J. Cree, Retinal vessel segmentation using the 2-d gabor wavelet and supervised classification, IEEE Transactions on Medical Imaging 25 (9) (2006) 1214–1222.

[51] C. A. Lupascu, D. Tegolo, E. Trucco, Fabc: retinal vessel segmentation using adaboost, IEEE Transactions on Information Technology in Biomedicine 14 (5) (2010) 1267–1274.

[52] X. You, Q. Peng, Y. Yuan, Y.-m. Cheung, J. Lei, Segmentation of retinal blood vessels using the radial projection and semi-supervised approach, Pattern Recognition 44 (10-11) (2011) 2314–2324.

[53] D. Marín, A. Aquino, M. E. Gegúndez-Arias, J. M. Bravo, A new supervised method for blood vessel segmentation in retinal images by using gray-level and moment invariants-based features, IEEE Transactions on Medical Imaging 30 (1) (2011) 146–158.

[54] Y. Wang, G. Ji, P. Lin, E. Trucco, Retinal vessel segmentation using multiwavelet kernels and multiscale hierarchical decomposition, Pattern Recognition 46 (8) (2013) 2117–2133.

[55] A. M. Mendonca, A. Campilho, Segmentation of retinal blood vessels by combining the detection of centerlines and morphological reconstruction, IEEE Transactions on Medical Imaging 25 (9) (2006) 1200–1213.

[56] M. A. Palomera-Pérez, M. E. Martinez-Perez, H. Benítez-Pérez, J. L. Ortega-Arjona, Parallel multiscale feature extraction and region growing: application in retinal blood vessel detection, IEEE Transactions on Information Technology in Biomedicine 14 (2) (2010) 500–506.

[57] M. E. Martinez-Perez, A. D. Hughes, S. A. Thom, A. A. Bharath, K. H. Parker, Segmentation of blood vessels from red-free and fluorescein retinal images, Medical Image Analysis 11 (1) (2007) 47–61.

[58] B. Al-Diri, A. Hunter, D. Steel, An active contour model for segmenting and measuring retinal vessels, IEEE Transactions on Medical Imaging 28 (9) (2009) 1488–1497.

[59] J. I. Orlando, M. Blaschko, Learning fully-connected crfs for blood vessel segmentation in retinal images, in: International Conference on Medical Image Computing and Computer-Assisted Intervention, 2014, pp. 634–641.

[60] G. Azzopardi, N. Strisciuglio, M. Vento, N. Petkov, Trainable cosfire filters for vessel delineation with application to retinal images, Medical Image Analysis 19 (1) (2015) 46–57.

[61] J. Zhang, B. Dashtbozorg, E. Bekkers, J. P. Pluim, R. Duits, B. M. ter Haar Romeny, Robust retinal vessel segmentation via locally adaptive derivative frames in orientation scores, IEEE Transactions on Medical Imaging 35 (12) (2016) 2631–2644.

[62] D. Goldberg, Genetic algorithm in search optimization and machine learing, addison-wesleypub (1989).

[63] M. Trzupek, M. R. Ogiela, R. Tadeusiewicz, Intelligent image content semantic description for cardiac 3D visualisations, Engineering Applications of Artificial Intelligence 24 (8) (2011) 1410–1418.

Cigdem Sazak received her B.S. degree in Computer Engineering from Sakarya University, Turkey, in 2011. She received his MSc degree in 2014 from Leicester University and is currently a PhD student in the Department of Computer Science at the University of Durham. Her research interests are in the image enhancement of biomedical images.

Carl J Nelson received a PhD in Computer Science from Durham University, UK in 2017. His research focused on the use of mathematical morphology for the analysis of bioimages. He is currently a research associate at the University of Glasgow, UK, where his interests focus on the interface of software and hardware for improved acquisition in light sheet microscopy.

Boguslaw Obara received a PhD in Computer Science from AGH, Poland. He has been a Fulbright fellow and a postdoctoral researcher at University California, USA and University of Oxford, UK. He is currently a professor in Computer Science at the Durham University, UK. His research focuses on image processing techniques.